DOI 10.2478/ama-2025-0036

# EVALUATION OF TENSILE STRESS RELAXATION OF SELECTIVE LASER SINTERING OF PA2200 MATERIAL USING THE MAXWELL-WIECHERT MODEL

**Wiktor SZOT[*], Mateusz RUDNIK[**], Paweł SZCZYGIEŁ[***], Natalia KOWALSKA[****]**

[*/***] Faculty of Mechatronics and Mechanical Engineering,
Department of Metrology and Unconventional Manufacturing Methods,
Kielce University of Technology, al. Tysiąclecia Państwa Polskiego 7 25-314 Kielce, Poland
[**/****] Faculty of Mechatronics and Mechanical Engineering,
Department of Fundamentals of Mechanical Engineering and Mechanical Technology,
Kielce University of Technology, al. Tysiąclecia Państwa Polskiego 7 25-314 Kielce, Poland

wszot@tu.kielce.pl, mrudnik@tu.kielce.pl, pszczygiel@tu.kielce.pl, nkowalska@tu.kielce.pl

*received 16 December 2024, revised 26 March 2025, accepted 14 April 2025*

**Abstract:** The use of 3D printing for the manufacture of functional components has led to a demand for research into the mechanical properties, including rheological properties, of additive manufactured models. In this article, the results of a study to evaluate the relaxation of tensile stress of samples made by selective laser sintering (SLS) of PA2200 material are presented. The evaluation of tensile stress relaxation was performed using the five-parameter Maxwell-Wiechert model. With the model used, elastic moduli and dynamic viscosity coefficients were calculated. The samples were made in three print orientations ($0°, 45°, 90°$) and two types of energy density ($E_d = 0.056\,J/mm^2$, $E_d = 0.076\,J/mm^2$). The results indicate that increasing the applied energy density leads to higher values of elastic moduli and dynamic viscosity coefficients. A strong fit of the model to the experimental curves was obtained, as confirmed by the obtained coefficients $Chi^2$ and $R^2$. This research comprehensively addresses the evaluation of the applicability of selective laser sintering technology, which is increasingly used in various areas of industry, as well as the influence of the process on the relaxation of tensile stress.

**Key words:** 3D printing, stress relaxation, Maxwell-Wiechert model, SLS

## 1. INTRODUCTION

Additive technology is one of the elements of Industry 4.0 [1]. Industry 4.0 also includes the process of testing technological and functional prototypes using 3D printing [1]. The testing of prototypes helps speed up the process of preparing the technological process for mass production [1]. In turn, testing of functional prototypes with properties similar to those of finished products enables a rapid and almost simultaneous refinement of the product at the prototype stage [1,2]. Testing involves, among other things, geometric analysis of the object through, for example, 3D scanning, and testing the mechanical properties (including rheological properties) of the functional prototype [3,4].

Studying the rheological properties of 3D printed parts is very important, if only because these parts can be subjected to long-term deformation or stress [5]. In the case of parts subjected to long-term deformation, one can speak of the phenomenon of stress relaxation [5,6]. Stress relaxation can be described using Maxwell's model as presented in several articles [7–14]. Maxwell models have different forms: simple and complex models, for example, models based on Prony series or models described by fractional calculus [13,14]. The stress relaxation of additively manufactured parts can vary depending on the print material used or the technological parameters of 3D printing, as confirmed in the articles [15,16].

In the article [7], the author conducted a study of stress relaxation of samples made by selective powder sintering (SLS) technology from PA 2200 material. Samples were produced setting values for two technological parameters: layer height (0.1 mm – 0.4 mm) and print orientation (0°, 90°). Stress relaxation was determined during uniaxial compression testing. The Maxwell-Wiechert model was used to describe the stress relaxation curves. The results showed a clear influence of layer height on stress relaxation. Additionally, it was shown that the orientation of the print affects stress relaxation.

In [17], the authors conducted stress relaxation tests on PLA material using fused deposition technology (FDM). The samples were produced using two technological parameters of the print: the orientation of the print (0°,45°, 90°) and the presence of a contour. In addition, the samples were subjected to different values of deformation and exposure to different temperatures during the tensile stress relaxation tests. To describe the stress-relaxation curves, 3 models were used: Maxwell, Findley and Linear solid. The results showed that Findley's law was the most appropriate empirical expression to predict the PLA tested. Stress distributions ranging from 11% to 14% were obtained. Both cooled and heated samples provided degradation of the quasistatic and long-term material properties. The presented results show the importance of stress relaxation effects in AM PLA structures.

In the article [11], the authors investigated, among other things, the stress relaxations of samples made of G6-Impact

nanocomposite using MEX material extrusion technology. The samples were made using the parameter of variable printing direction (0/45/-45/90/90/-45/45/0). The following were carried out: tensile stress relaxations, bending stress relaxations and compressive stress relaxations. On the basis of the results, it was found that the bending mode had the lowest relaxation, while the highest relaxation was observed for the tensile mode.

The viscoelastic behaviour of the materials strongly influences their application area [18,19]. The literature review presented above shows that the viscoelastic behaviour of 3D printed polymers depends on factors such as material type, 3D printing process, and type of load [2,10,20,21]. However, due to the limited number of studies in the field of stress relaxation of 3D printed materials, there is a need for continuous expansion to better understand this phenomenon.

Consequently, the purpose of the article was to determine the elastic moduli and dynamic viscosity coefficients of the PA 2200 polymer material. This material is well suited for medical devices such as orthoses or biomodels. The calculations used the five-parameter Maxwell-Wiechert model to determine the stress relaxation in the material. This research is very important because the calculated coefficients and modulus can be used in engineering calculations.

## 2. MATERIAL AND METHODS

### 2.1. Material PA2200

The test samples were made from PA 2200, This material is a powdered whitish fine polyamide. Prints made from polyamide powder have good mechanical properties, stiffness, and chemical resistance, similar to those of other materials used in industrial applications [20,22]. Table 1 focusses on the properties of PA 2200 as given by the manufacturer (EOS GmbH, Krailling, Germany) [23].

**Tab. 1.** Properties of PA 2200 powder [23]

| **Powder properties** | | **Value** | **Unit** | **Test Standard** |
|---|---|---|---|---|
| Medium grain size | | 60 | µm | - |
| Density of ubound powder | | 0.435 – 0.445 | $g/cm^3$ | DIN 53466 |
| Density of sintered powder | | 0.9 – 0.95 | $g/cm^3$ | EOS - Method |
| **Mechanical Properties** | | **Value** | **Unit** | **Test Standard** |
| Flexural modulus, 23°C | | 1500 | MPa | ISO 178 |
| Flexural strength | | 58 | | ISO 178 |
| Izod impact notched, 23°C | | 4.4 | $kJ/m^2$ | ISO 180/1A |
| Izod impact unnotched, 23°C | | 32.8 | | ISO 180/1U |
| Shore D hardness (15 s) | | 75 | ------ | ISO 868 |
| Ball indentation hardness | | 78 | MPa | ISO 2039-1 |
| **3D Data** | | **Value** | **Unit** | **Test Standard** |
| Tensile modulus | X-direction | 700 | MPa | ISO 527-1/-2 |
| | Y-direction | 1700 | | |
| | Z-direction | 1650 | | |
| Tensile strength | X-direction | 48 | | |
| | Y-direction | 48 | | |
| | Z-direction | 47 | | |
| Strain at break | X-direction | 24 | % | ISO 527-1/-2 |
| Charpy impact strength (+23°C) | X-direction | 53 | $kJ/m^2$ | ISO 179/1eU |
| Charpy notched impact strength (+23°C) | X-direction | 4.8 | | ISO 179/1eA |
| Thermal conductivity | X-direction | 0.144 | W/(mK) | DIN 52616 |
| | Y-direction | 0.144 | | |
| | Z-direction | 0.127 | | |

The PA 2200 material is biocompatible according to EN ISO 10993-1 and is USP / level VI / 121°C and approved for food contact according to the European Directive 2002/72/EC (except for alcoholic products) [23]. This polyamide can be used to manufacture consumer parts, medical devices, and functional plastic parts [2].

### 2.2. SLS technology

In the presented research, the well-known Formiga P100 machine (EOS GmbH, Krailling, Germany), which realises selective laser sintering - SLS technology, was used to build models. This machine makes it possible to produce physical plastic-based models with dimensions that do not exceed the dimensions of the working chamber of 250 mm x 200 mm x 330 mm. In the mentioned technology, a $CO_2$ laser is very often used to sinter the input material in the form of powder. The entire technological process is performed in an inert gas. The production scheme using SLS technology is shown in Figure 1 [2,24,25].

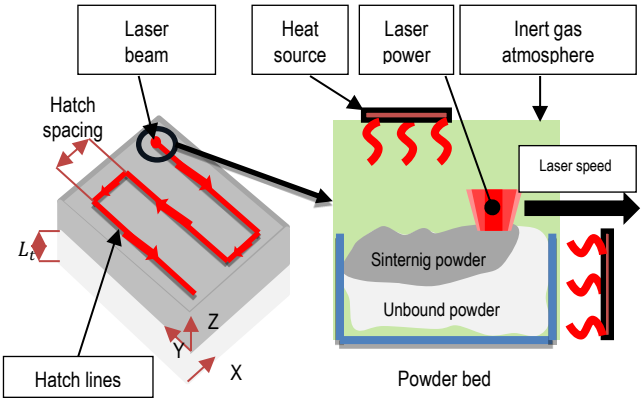


**Fig. 1.** Principle of SLS technology [2]

Fig. 1 also provides an explanation of the technological parameters in SLS technology such as layer thickness $L_t$, hatch spacing, laserpower and laser speed.

### 2.3. Samples Preparation

The test samples were designed in SolidWorks according to ISO 527. The shape of the samples are paddles with the dimensions in millimeters shown in Figure 2(a).

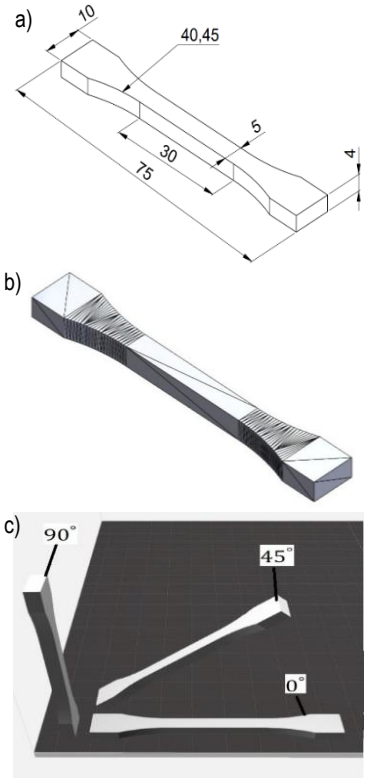


**Fig. 2.** Test specimens: a) dimensions, b) STL saving, c) print orientation

The STL files of the samples were saved with the following approximation parameters: linear tolerance of 0.007 mm and angular tolerance of 5°. The appearance of the sample in the STL record is shown in Figure 2(b). Six types of samples were produced with different 3D printing technological parameters, each variant was parted 10 times to account for statistical calculations.

The analysed technological parameters of 3D printing were energy density $E_d$, print orientation $P_d$ and layer height $L_t$ whose values are shown in Table 2. Interpretations of the positioning of the samples on the work platform are shown in Figure 2(c).

**Tab. 2.** Values of technological parameters

| $\mathbf{E_d}$ | | $\mathbf{P_d}$ | $\mathbf{L_t}$ |
|---|---|---|---|
| 0.056 J/mm$^2$ | 0.076 J/mm$^2$ | 0°, 45°, 90° | 0.1 mm |
| P = 21 W | P = 22 W | | |
| v = 2500 mm/s | v = 1970 mm/s | | |

The energy density $E_d$ transferred to the sintered layer was calculated using Equation 1 [5,24]:

$$E_d = \frac{P}{vh}\chi \quad (1)$$

where: $P$ – laser power, $W$; $v$ – laser beam speed, mm/s.; $h$ = 0.25 mm (distance between successive laser beams); $d$ = 0.42 mm (diameter of focused beam); $x$ = 1.68 (overlap factor).

Each individual sample was labelled according to the formula: $E_d^{56} - P_d^0 - 1$, which means $E_d^{56}$ – energy density, $P_d^0$ – print orientations, 1 – sample number.

### 2.4. The Maxwell-Wiechert model

A complex five-parameter Maxwell-Wiechert model was used to describe the stress relaxation curves obtained from the stress relaxation tests. Approximations of this model to experimental curves were carried out with the OriginPro software using the Levenberg-Marquardt algorithm. The mechanical analogy of the Maxwell-Wiechert five-parameter model is shown in Figure 3 [5,13].

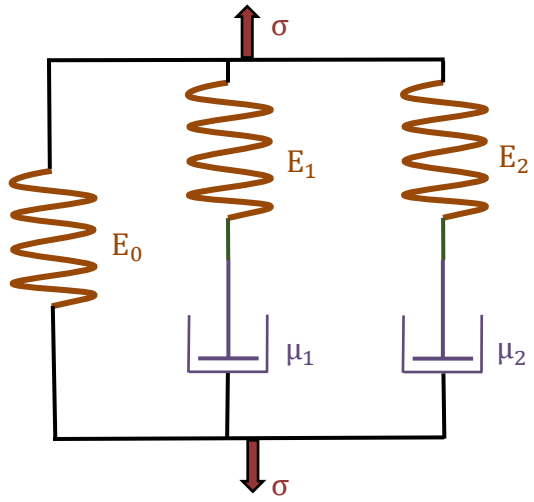


**Fig. 3.** Mechanical analogy of the Maxwell-Wiechert model [5,13]

The equation describing the Maxwell-Wiechert model consisting of five parameters is as follows [5,13]:

$$\sigma(t) = \sigma_0 + \sigma_1 e^{\frac{-t}{t_1}} + \sigma_2 e^{\frac{-t}{t_2}} \quad (2)$$

where $t_1$, $t_2$ are there relaxation times (s) of each model:

$$t_1 = \frac{\mu_1}{E_1},\ t_2 = \frac{\mu_2}{E_2} \quad (3)$$

After transforming equations (2) and (3), an equation was obtained describing the five-parameter Maxwell-Wiechert model, including all the parameters of this model [5,13].

$$\sigma(t) = \varepsilon_0 \left( E_0 + E_1 e^{\frac{-E_1 t}{\mu_1}} + E_2 e^{\frac{-E_2 t}{\mu_2}} \right) \quad (4)$$

where: $\varepsilon_0$ – unit initial strain; $E_0$, $E_1$, $E_2$ – moduli of elasticity, MPa; $\mu_1$, $\mu_2$ – coefficients of dynamic viscosity, MPa; $t$ – time, s.

The equivalent modulus was also calculated using the following formula [5,13]:

$$E_s = E_0 + E_1 + E_2 \quad (5)$$

where: $E_0$, $E_1$, $E_2$ – moduli of elasticity, MPa.

The decrease in stress after time t was calculated using the formula [5,13]:

$$R_\sigma = \frac{\sigma_0 - \sigma_t}{\sigma_0} \cdot 100\% \quad (6)$$

where: $\sigma_0$ – initial stress, MPa; $\sigma_t$ – stress after time t, MPa.

### 2.5. Measurement technologies

Stress relaxation tests were conducted using a Hegewald & Peschke Inspekt 3kN testing machine. The test parameters used to conduct the stress relaxation tests were: preload $F_p = 100\ N$, speed of displacement of the machine crossbar to achieve the set strain $v_{mm} = 10\ mm/s$, permanent strain $\varepsilon_0 = 0.02$, test duration $t = 600\ s$. The test specimens were subjected to tensile stress, as can be seen in Figure 4.

**Fig. 4.** Appearance of samples during stress relaxation tests

The test samples were exposed to tensile stresses.

## 3. RESULTS

Stress relaxation tests were performed, resulting in stress relaxation curves. These curves are shown in Figures 5 and 6.

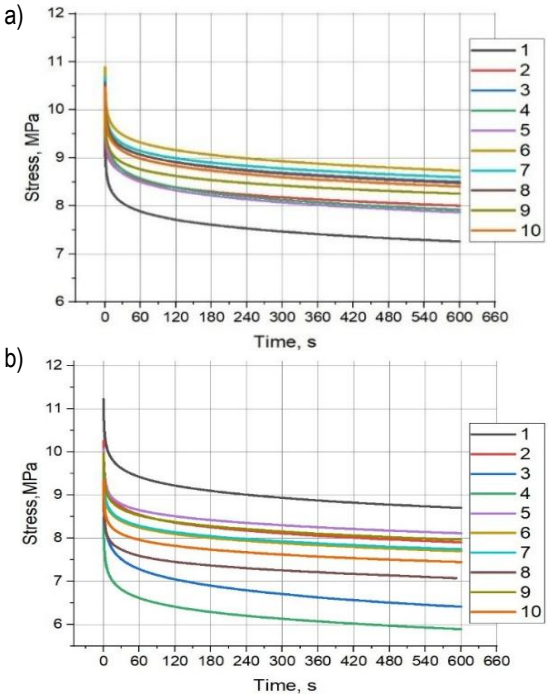


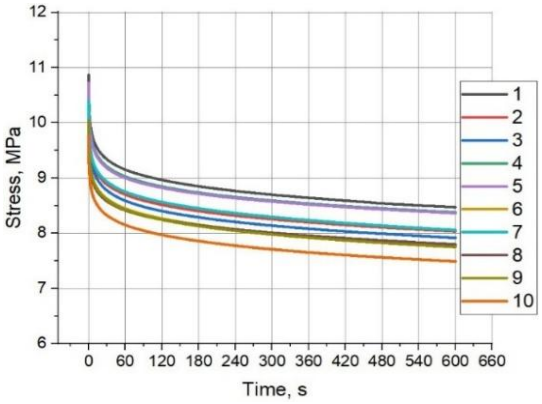


**Fig. 5.** Stress relaxation curves for PA2200 material; $E_d^{56}$: a) $E_d^{56} - P_d^0$, b) $E_d^{56} - P_d^{45}$, c) $E_d^{56} - P_d^{90}$

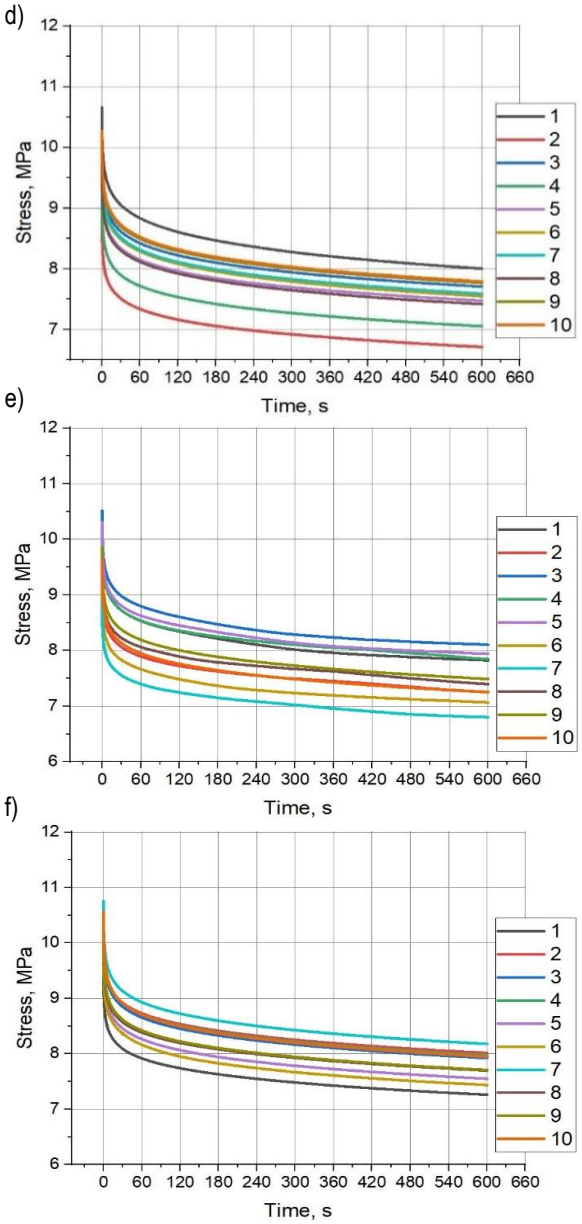


**Fig. 6.** Stress relaxation curves for PA2200 material: d) $E_d^{76} - P_d^0$, e) $E_d^{76} - P_d^{45}$, f) $E_d^{76} - P_d^{90}$

For each individual curve, a five-parameter Maxwell-Wiechert model was approximated using the Levenberg-Marquardt algorithm. An example of the appearance of these fits for selected relaxation curves is shown in Figure 7.

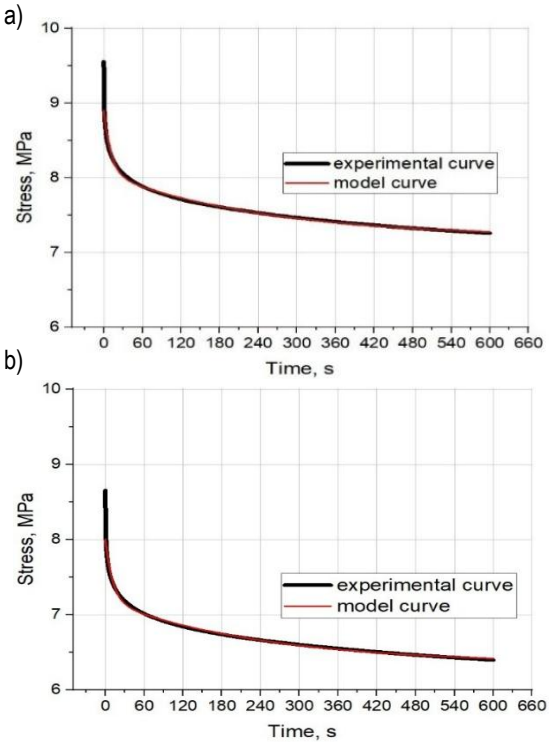


**Fig. 7.** Example of a Maxwell-Wiechert model fit to experimental curves: a) $E_d^{56} - P_d^0 - 1$, b) $E_d^{76} - P_d^0 - 1$

As a result of fitting of the five-parameter Maxwell-Wiechert model with five parameters to the stress relaxation curves, the values of model parameters $\sigma_0$, $\sigma_1$, $\sigma_2$, $t_1$, $t_2$ and fitting coefficients $Chi^2$, $R^2$ were obtained. The values of these parameters and welding coefficients were separated into two tables 3, 4 due to the energy density of the technological 3D printing parameter energy density occurring in two values $E_d = 0.056\,J/mm^2$ and $E_d = 0.076\,J/mm^2$.

**Tab. 3.** Maxwell-Wichert model parameters and fit coefficients; $\mathrm{E_d^{56}}$

| Lp. | $\sigma_0$, MPa | $\sigma_1$, MPa | $\sigma_2$, MPa | $t_1$, s | $t_2$, s | $Chi^2$ | $R^2$ |
|---|---|---|---|---|---|---|---|
| $\mathbf{P_d^0}$ | | | | | | | |
| **1** | 7.8 | 0.9 | 0.8 | 11 | 232 | 0.000390 | 0.9942 |
| **2** | 8.4 | 0.7 | 0.8 | 10 | 252 | 0.000299 | 0.9945 |
| **3** | 8.4 | 0.7 | 0.8 | 10 | 239 | 0.000314 | 0.9947 |
| **4** | 7.9 | 0.9 | 0.9 | 11 | 233 | 0.000403 | 0.9947 |
| **5** | 7.8 | 0.8 | 0.9 | 11 | 241 | 0.000369 | 0.9948 |
| **6** | 8.7 | 0.8 | 0.8 | 11 | 252 | 0.000348 | 0.9942 |
| **7** | 8.5 | 0.8 | 0.7 | 11 | 247 | 0.000337 | 0.9937 |
| **8** | 8.2 | 0.7 | 0.7 | 11 | 251 | 0.000267 | 0.9941 |
| **9** | 8.3 | 0.7 | 0.8 | 11 | 255 | 0.000299 | 0.9949 |
| **10** | 8.0 | 0.7 | 0.7 | 11 | 240 | 0.000309 | 0.9938 |
| $\bar{x}$ | 8.2 | 0.8 | 0.8 | 11 | 244 | 0.000334 | 0.9944 |
| ***SD*** | 0.3 | 0.1 | 0.1 | 0.3 | 8 | 0.000044 | 0.0004 |
| $\mathbf{P_d^{45}}$ | | | | | | | |
| 1 | 8.6 | 0.9 | 1.0 | 12 | 243 | 0.000445 | 0.9951 |
| 2 | 7.9 | 0.9 | 0.9 | 11 | 241 | 0.000410 | 0.9944 |
| 3 | 6.3 | 1.0 | 1.2 | 12 | 263 | 0.000544 | 0.9958 |
| 4 | 5.8 | 1.0 | 1.0 | 12 | 249 | 0.000512 | 0.9944 |
| 5 | 8.1 | 0.7 | 0.7 | 11 | 267 | 0.000279 | 0.9943 |
| 6 | 7.6 | 0.7 | 0.7 | 11 | 259 | 0.000304 | 0.9941 |
| 7 | 7.7 | 0.7 | 0.7 | 11 | 252 | 0.000332 | 0.9936 |
| 8 | 7.0 | 0.7 | 0.7 | 10 | 264 | 0.000326 | 0.9930 |
| 9 | 7.9 | 0.7 | 0.8 | 11 | 258 | 0.000292 | 0.9947 |
| 10 | 7.4 | 0.7 | 0.7 | 10 | 249 | 0.000264 | 0.9943 |
| $\bar{x}$ | 7.4 | 0.8 | 0.8 | 11 | 255 | 0.000371 | 0.9944 |
| ***SD*** | 0.8 | 0.1 | 0.2 | 1 | 9 | 0.000101 | 0.0008 |
| $\mathbf{P_d^{90}}$ | | | | | | | |
| 1 | 8.4 | 0.9 | 0.9 | 12 | 257 | 0.000421 | 0.9948 |
| 2 | 8.0 | 0.9 | 0.9 | 11 | 245 | 0.000424 | 0.9945 |
| 3 | 7.9 | 0.9 | 0.9 | 11 | 245 | 0.000433 | 0.9945 |
| 4 | 8.3 | 0.9 | 0.9 | 12 | 242 | 0.000393 | 0.9947 |
| 5 | 8.3 | 0.9 | 0.9 | 11 | 245 | 0.000408 | 0.9944 |
| 6 | 7.7 | 0.8 | 0.9 | 12 | 262 | 0.000367 | 0.9952 |
| 7 | 7.9 | 0.8 | 0.9 | 12 | 253 | 0.000369 | 0.9954 |
| 8 | 7.7 | 0.8 | 0.8 | 11 | 260 | 0.000364 | 0.9944 |
| 9 | 7.7 | 0.8 | 0.9 | 12 | 262 | 0.000353 | 0.9954 |
| 10 | 8.0 | 0.8 | 0.9 | 12 | 268 | 0.000391 | 0.9952 |
| $\bar{x}$ | 8.0 | 0.8 | 0.9 | 12 | 254 | 0.000392 | 0.9948 |
| ***SD*** | 0.3 | 0.04 | 0.03 | 0.3 | 9 | 0.000028 | 0.0004 |

Based on Table 3, high standard deviation values of standard deviations can be seen for $t_2$ relaxation times. Low standard

DOI 10.2478/ama-2025-0036


deviation values were obtained for the other parameters of the Maxwell-Wiechert model and the fit coefficients $Chi^2$, $R^2$.

**Tab. 4.** Maxwell-Wichert model parameters and fit coefficients; $E_d^{76}$

| Lp. | $\sigma_0$, MPa | $\sigma_1$, MPa | $\sigma_2$, MPa | $t_1$, s | $t_2$, s | $Chi^2$ | $R^2$ |
|---|---|---|---|---|---|---|---|
| $P_d^0$ | | | | | | | |
| 1 | 7.9 | 0.9 | 1.1 | 13 | 255 | 0.000464 | 0.9960 |
| 2 | 6.7 | 0.8 | 0.8 | 12 | 251 | 0.000377 | 0.9945 |
| 3 | 7.6 | 0.9 | 1.0 | 12 | 249 | 0.000404 | 0.9954 |
| 4 | 7.0 | 0.8 | 0.9 | 11 | 242 | 0.000382 | 0.9950 |
| 5 | 7.4 | 0.9 | 0.9 | 12 | 243 | 0.000425 | 0.9947 |
| 6 | 7.5 | 0.9 | 1.0 | 12 | 248 | 0.000412 | 0.9956 |
| 7 | 7.5 | 0.9 | 1.0 | 12 | 251 | 0.000439 | 0.9952 |
| 8 | 7.7 | 0.9 | 1.0 | 12 | 245 | 0.000434 | 0.9953 |
| 9 | 7.4 | 0.9 | 1.0 | 11 | 244 | 0.000402 | 0.9952 |
| 10 | 7.7 | 0.9 | 1.0 | 13 | 246 | 0.000434 | 0.9953 |
| $\bar{x}$ | 7.4 | 0.9 | 1.0 | 12 | 247 | 0.000418 | 0.9952 |
| $SD$ | 0.4 | 0.03 | 0.1 | 1 | 4 | 0.000027 | 0.0004 |
| $P_d^{45}$ | | | | | | | |
| 1 | 7.8 | 0.9 | 1.0 | 9 | 209 | 0.000264 | 0.9971 |
| 2 | 7.1 | 0.8 | 0.9 | 14 | 337 | 0.000558 | 0.9917 |
| 3 | 8.1 | 0.9 | 1.0 | 8 | 193 | 0.000226 | 0.9974 |
| 4 | 7.7 | 0.9 | 0.9 | 14 | 314 | 0.000579 | 0.9925 |
| 5 | 7.9 | 0.9 | 1.0 | 9 | 224 | 0.000252 | 0.9970 |
| 6 | 7.1 | 0.8 | 0.8 | 9 | 182 | 0.000303 | 0.9953 |
| 7 | 6.7 | 0.8 | 0.9 | 13 | 330 | 0.000343 | 0.9945 |
| 8 | 7.1 | 0.8 | 1.0 | 17 | 464 | 0.000635 | 0.9908 |
| 9 | 7.4 | 0.8 | 1.0 | 12 | 264 | 0.000395 | 0.9953 |
| 10 | 7.2 | 0.8 | 1.0 | 12 | 257 | 0.000394 | 0.9952 |
| $\bar{x}$ | 7.4 | 0.8 | 0.9 | 12 | 277 | 0.000395 | 0.9947 |
| $SD$ | 0.4 | 0.04 | 0.1 | 3 | 86 | 0.000147 | 0.0023 |
| $P_d^{90}$ | | | | | | | |
| 1 | 7.2 | 0.8 | 0.9 | 12 | 258 | 0.000373 | 0.9949 |
| 2 | 7.9 | 0.9 | 1.0 | 11 | 252 | 0.000415 | 0.9953 |
| 3 | 7.9 | 0.9 | 1.0 | 12 | 253 | 0.000446 | 0.9952 |
| 4 | 7.9 | 0.9 | 1.0 | 12 | 253 | 0.000430 | 0.9954 |
| 5 | 7.5 | 0.9 | 1.0 | 12 | 244 | 0.000415 | 0.9953 |
| 6 | 7.4 | 0.9 | 1.0 | 13 | 239 | 0.000444 | 0.9951 |
| 7 | 8.1 | 0.9 | 1.0 | 12 | 250 | 0.000458 | 0.9953 |
| 8 | 7.6 | 0.9 | 0.9 | 11 | 251 | 0.000414 | 0.9949 |
| 9 | 7.6 | 0.9 | 1.0 | 12 | 253 | 0.000430 | 0.9951 |
| 10 | 7.9 | 1.0 | 1.0 | 12 | 248 | 0.000482 | 0.9951 |
| $\bar{x}$ | 7.7 | 0.9 | 1.0 | 12 | 250 | 0.000431 | 0.9952 |
| $SD$ | 0.3 | 0.04 | 0.04 | 0.4 | 5 | 0.000029 | 0.0001 |

Analysing the data collected in Table 4, high values of standard deviations can be observed for the $t_2$ relaxation times. Low standard deviation values were obtained for the other parameters of the Maxwell-Wiechert model and fit coefficients $Chi^2$, $R^2$.

Based on the average values of the Maxwell-Wiechert model parameters $\bar{\sigma}_0$, $\bar{\sigma}_1$, $\bar{\sigma}_2$, $\bar{t}_1$, $\bar{t}_2$ and the values of the constant strain $\varepsilon_0 = 1\ mm$, using formulas (2), (3) and (4), the elastic moduli $E_0$, $E_1$, $E_2$ and the dynamic viscosity coefficients $\mu_1$, $\mu_2$ were calculated. The values of these moduli and coefficients are shown in Figures 8, 9. Furthermore, using formula (5), the equivalent modulus $E_s$ was calculated, which is also shown in Figure 8.

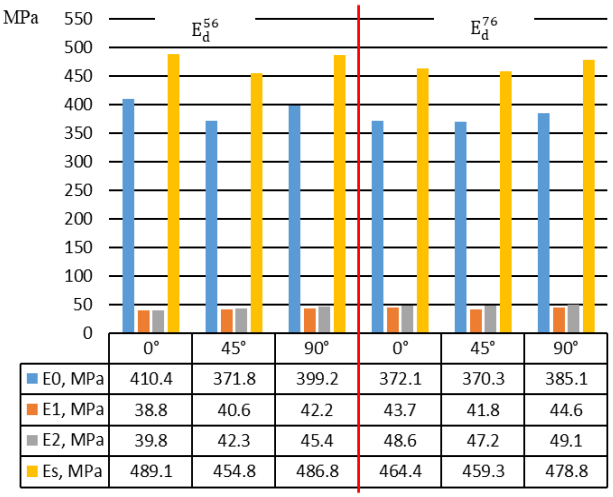


| | 0° | 45° | 90° | 0° | 45° | 90° |
|---|---|---|---|---|---|---|
| E0, MPa | 410.4 | 371.8 | 399.2 | 372.1 | 370.3 | 385.1 |
| E1, MPa | 38.8 | 40.6 | 42.2 | 43.7 | 41.8 | 44.6 |
| E2, MPa | 39.8 | 42.3 | 45.4 | 48.6 | 47.2 | 49.1 |
| Es, MPa | 489.1 | 454.8 | 486.8 | 464.4 | 459.3 | 478.8 |

**Fig. 8.** Moduli of elasticity for PA 2200 material

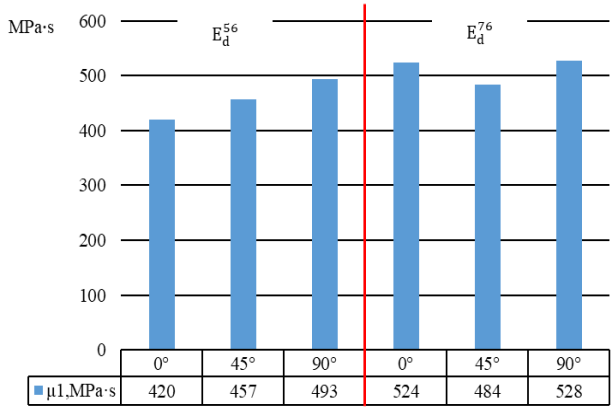


| | 0° | 45° | 90° | 0° | 45° | 90° |
|---|---|---|---|---|---|---|
| μ1,MPa·s | 420 | 457 | 493 | 524 | 484 | 528 |

DOI 10.2478/ama-2025-0036

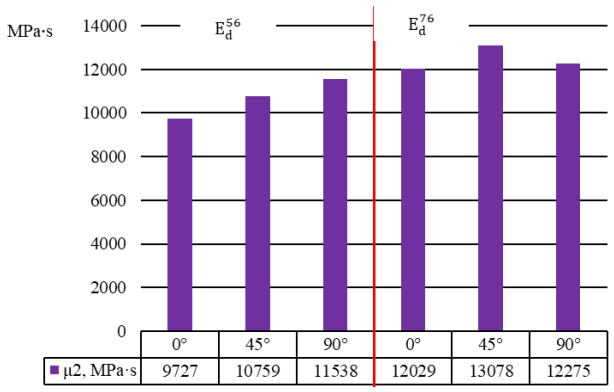


**Fig. 9.** Dynamic viscosity coefficients for PA 2200 material

The stress relaxation curves obtained from the tests were used to calculate, according to Equation (6), the percentage decrease in stress $R_\sigma$ after time t. The values of the percentage decrease in stress $R_\sigma$ are shown in Table 5.

In the data in the table above, it is evident that the highest decrease in stress occurred for $E_d^{56}$ and $P_d^{45}$. While the lowest decrease in stress was for $E_d^{56}$ and $P_d^0$.

**Tab. 5.** Percentage of stress drop in PA2200 material

| $R_\sigma$, % | | | |
|---|---|---|---|
| $E_d^{56}$ | | | |
| $P_d$ | $0^\circ$ | $45^\circ$ | $90^\circ$ |
| $\bar{x}$ | 20.98 | 23.85 | 22.61 |
| SD | 1.86 | 4.86 | 0.56 |
| $E_d^{76}$ | | | |
| $\bar{x}$ | 24.5 | 23.6 | 24.1 |
| SD | 0.4 | 0.5 | 0.4 |

In the data in the table above, it is evident that the highest decrease in stress occurred for $E_d^{56}$ and $P_d^{45}$. While the lowest decrease in stress was for $E_d^{56}$ and $P_d^0$.

## 4. DISCUSSION

The translation of stress relaxation curves seen in Figures 5 and 6, and particularly noticeable for samples printed according to technological parameters $E_d^{56} - P_d^{45}$ may be due to the difficulty of realising a unit stress stroke. The unit stress stroke is performed at the highest possible speed, which is difficult to perform under laboratory conditions. Also, the difficulty of setting a pre-stress for each individual specimen, can cause an apparent translation of test results. Too high values of pre-stress will cause the specimen to begin relaxing stresses even before the test begins, while too low values will lead to a stress stroke that is not correct to achieve the set strain.

Based on Figure 7, the Maxwell-Wiechert fit of the five-parameter model to the stress relaxation curves is strong. This can be concluded not only from a visual assessment of Figure 7 (the red line overlaps with the black line), but also by turning our attention to the values of the $Chi^2$ fit test coefficients and $R^2$ determination coefficients shown in Tables 3 and 4. It should be mentioned here that the $R^2$ determination coefficient always varies between '0' and "1" and is a measure of the fit of the regression equation $R^2$ values close to "1", i.e. those shown in Tables 3 and 4, indicate that the regression equation is very useful to predict the value of the dependent variable Y with the independent variable X. For the $Chi^2$ concordance test, values close to '0' indicate a strong model fit.

The high standard deviation values for the stress relaxation time $t_2$ (Table 3 and 4) may be related to dynamic viscosity. The dynamic viscosity, on the other hand, depends on the structure at the molecular level of the material in this case PA 2200, which is a polymer. Polymers are made up of long polymer chains that form numerous intermolecular interactions.

When analysing the data in Figures 8 and 9, that is, the elastic moduli $E_0$, $E_1$, $E_2$ and the dynamic viscosity coefficients $\mu_1$, $\mu_2$, one can see a slight anisotropy of the stress relaxation properties due to the orientations of the print.

Analysing the elastic moduli $E_0$, $E_1$, $E_2$ p shown in Figure 8, it can be concluded that, there are differences within the same direction, e.g. the modulus of $E_0$ is many times greater than the moduli of $E_1$, $E_2$. This regularity informs that in terms of viscoelastic properties the material produced by selective laser sintering technology can be quasi-isotropic.

Analysing the different print orientations $0^\circ$, $45^\circ$, $90^\circ$ for the equivalent moduli $E_s$ and dynamic viscosity coefficients $\mu_1$, $\mu_2$ shown in Figures 8 and 9, it can be seen that there is a difference in values between the applied energy densities $E_d = 0.056\ J/mm^2$ and $E_d = 0.076\ J/mm^2$. The equivalent moduli of $E_s$ for print orientations $0^\circ$, $90^\circ$ and energy density $E_d^{56}$ are 5% and 2% larger, respectively, than the same equivalent moduli and print orientation, but for energy density $E_d^{76}$. The value of the equivalent modulus $E_s$ with print orientation $45^\circ$ and $E_d^{56}$ was 1% smaller than the same modulus for the same print orientation but energy density $E_d^{76}$. For dynamic viscosity coefficient $\mu_1$ the differences between the energy densities for print orientations $0^\circ$, $45^\circ$, $90^\circ$ were 20%, 6%, 7%, respectively, in favor of energy density $E_d^{76}$ or dynamic viscosity coefficient $0^\circ$, $45^\circ$, $90^\circ$ the differences between energy densities for print orientations $E_d^{76}$.

However, for energy density $E_d^{76}$ and print orientations $0^\circ$, $90^\circ$ the values of percentage stress drop values are higher by 14%, 6%, respectively, compared to the same orientations but for lower energy density $E_d^{56}$. In contrast, for print orientation $45^\circ$, the value of percentage stress drop for energy density $E_d^{56}$ was 1% higher than the same value but for energy density $E_d^{76}$.

## 5. CONCLUSSIONS

On the basis of the results of the stress relaxation tests, the following general conclusions can be drawn:

- A strong fit of the Maxwell-Wiechert model to the stress relaxation curves, confirmed by the values of the $Chi^2$ consistency and $R^2$ determination test coefficients.
- A small anisotropy of rheological properties was detected due to the orientation of the print.
- Increasing the energy density from $0.056\ J/mm^2$ to $0.076\ J/mm^2$, or the equivalent modulus $E_s$, it increases in $0^\circ$, $90^\circ$ orientations. The opposite is true for this modulus in the case of $45^\circ$ print orientation.
- Increasing the energy densities from $0.056\ J/mm^2$ to $0.076\ J/mm^2$ also increases the values of dynamic viscosity coefficients $\mu_1$, $\mu_2$ in the $0^\circ$ ($9727\ MPa \cdot s \uparrow 12029\ MPa \cdot s$), $45^\circ$ ($10759\ MPa \cdot s \uparrow 13078\ MPa \cdot$

s) ,$90^{\circ}$ ($11539\ \mathrm{MPa}\cdot\mathrm{s} \uparrow 12275\ \mathrm{MPa}\cdot\mathrm{s}$) print orientations.

– Increasing the energy densities from $0.056\,J/mm^2$ to $0.076\,J/mm^2$ also increases the values of the percentage stress drop $\mathrm{R}_{\sigma}$ in the $0^{\circ}$ ($20.98\% \uparrow 24.5\%$), $90^{\circ}$($22.61\% \uparrow 24.1\%$) print orientations. In the case of $45^{\circ}$ ($23.85\% \downarrow 23.6\%$) print orientation, the trend is reversed.

The calculated values of the elastic moduli $\mathrm{E}_0$, $\mathrm{E}_1$, $\mathrm{E}_2$ and dynamic viscosity coefficients $\mu_1$, $\mu_2$ can be used to model components produced by selective powder sintering (SLS) technology from PA2200 material. In particular, the application of these moduli and dynamic viscosity coefficients can be found in engineering calculations.

## REFERENCES

1. Oleksy M, Budzik G, Sanocka-Zajdel A, Paszkiewicz A, Bolanowski M, Oliwa R, et al. Industry 4.0 Part I. Selected applications in processing of polymer materials. Polimery/Polymers. 2018;63(7–8):531–5.
2. Dincă (Shamieh) LL, Popa NM, Milodin NL, Stanca C, Gheorghiu D. Influence of the process parameters on mechanical properties of the final parts obtained by selective laser sintering from PA2200 powder. MATEC Web of Conferences. 2019;299:01001.
3. Malashin I, Martysyuk D, Tynchenko V, Nelyub V, Borodulin A, Galinovsky A. Mechanical Testing of Selective-Laser-Sintered Polyamide PA2200 Details: Analysis of Tensile Properties via Finite Element Method and Machine Learning Approaches. Polymers (Basel). 2024 Mar 1;16(6).
4. Eftekhari M, Fatemi A. On the strengthening effect of increasing cycling frequency on fatigue behavior of some polymers and their composites: Experiments and modeling. Int J Fatigue. 2016 Jun 1;87:153–66.
5. Szot W, Bochnia J, Zmarzły P. Effect of selective laser sintering on stress relaxation in PA12. In: Polimery/Polymers. Industrial Chemistry Research Institute; 2024. p. 179–85.
6. Szot W, Rudnik M. Effect of the Number of Shells on Selected Mechanical Properties of Parts Manufactured by FDM/FFF Technology. Advances in Materials Science. 2024 Mar 1;24(1):86–103.
7. Kozior T. Rheological properties of polyamide pa 2200 in sls technology. Tehnicki Vjesnik. 2020 Aug 1;27(4):1092–100.
8. Nam TH, Petríková I, Marvalová B. Stress relaxation behavior of isotropic and anisotropic magnetorheological elastomers. Continuum Mechanics and Thermodynamics. 2024 Mar 1;36(2):299–315.
9. Obaid N, Kortschot MT, Sain M. Understanding the stress relaxation behavior of polymers reinforced with short elastic fibers. Materials. 2017;10(5).
10. Ye J, Yao T, Deng Z, Zhang K, Dai S, Liu X. A modified creep model of polylactic acid (PLA-max) materials with different printing angles processed by fused filament fabrication. J Appl Polym Sci. 2021 May 5;138(17).
11. Reis PNB, Valvez S, Ferreira JAM. Creep and stress relaxation behaviour of 3D printed nanocomposites. In: Procedia Structural Integrity. Elsevier B.V.; 2022. p. 934–40.
12. Kozior T, Kundera C. Rheological properties of cellular structures manufactured by additive PJM technology. Tehnicki Vjesnik. 2021;28(1):82–7.
13. Bochnia J. Evaluation of relaxation properties of digital materials obtained by means of PolyJet Matrix technology. Bulletin of the Polish Academy of Sciences: Technical Sciences. 2018;66(6):891–7.
14. Bochnia J, Blasiak S. Stress relaxation and creep of a polymer-aluminum composite produced through selective laser sintering. Polymers (Basel). 2020 Apr 1;12(4).
15. Aberoumand M, Rahmatabadi D, Soltanmohammadi K, Soleyman E, Ghasemi I, Baniassadi M, et al. Stress recovery and stress relaxation behaviors of PVC 4D printed by FDM technology for high-performance actuation applications. Sens Actuators A Phys. 2023 Oct 16;361.
16. Jang JW, Min KE, Kim C, Wern C, Yi S. Rheological Properties and 3D Printing Behavior of PCL and DMSO2 Composites for Bio-Scaffold. Materials. 2024 May 1;17(10).
17. Bertocco A, Bruno M, Armentani E, Esposito L, Perrella M. Stress Relaxation Behavior of Additively Manufactured Polylactic Acid (PLA). Materials. 2022 May 1;15(10).
18. Wang X, Zhou M, Bai J, Liao Y, Li D, Zhang B. Research on the Rheological Properties and Diffusion Law of Coal-Based Solid Waste Geopolymer Grouting Material. Materials [Internet]. 2024 Nov 7;17(22):5433. Available from: https://www.mdpi.com/1996-1944/17/22/5433
19. Tüfekci K, Çakan BG, Küçükakarsu VM. Stress relaxation of 3D printed PLA of various infill orientations under tensile and bending loadings. J Appl Polym Sci. 2023 Oct 15;140(39).
20. Singh S, Kaur D, Singh M, Balu R, Mehta A, Vasudev H. Challenges and issues in manufacturing of components using polymer-based selective laser sintering (SLS): a review. International Journal on Interactive Design and Manufacturing. 2024;
21. Chen J, Kong Y, Lu K, Huang Q. A Computational Solid Mechanics analysis on the supportability of 3D 2 printing surimi depended on creep and stress relaxation [Internet]. Available from: https://ssrn.com/abstract=4956847
22. Jabri FE, Ouballouch A, Lasri L, Alaiji R El. A comprehensive review of polymer materials and selective laser sintering technology for 3D printing. Vol. 118, Journal of Achievements in Materials and Manufacturing Engineering. International OCSCO World Press; 2023. p. 5–17.
23. EOS GmbH. Material data sheet PA 2200 [Internet]. Krailling: EOS GmbH Electro Optical Systems; [cited 2025 May 14]. Available from: https://www.eos.info/polymer-solutions/polymer-materials/data-sheets/mds-pa-2200-balance
24. Liu K. Effect of process parameters on the temperature field of laser sintering of nylon PA2200 powder. In: Journal of Physics: Conference Series. Institute of Physics; 2024.
25. Faes M, Wang Y, Lava P, Moens D. Variability, heterogeneity, and anisotropy in the quasi-static response of laser sintered PA12 components. Strain. 2017 Apr 1;53(2).

Wiktor Szot: https://orcid.org/0000-0001-9512-9680
Mateusz Rudnik: https://orcid.org/0000-0001-5096-608X
Paweł Szczygieł: https://orcid.org/0000-0002-3113-3557
Natalia Kowalska: https://orcid.org/0000-0003-3043-7812